



# Graphene FET Array Biosensor Based on ssDNA Aptamer for Ultrasensitive Hg<sup>2+</sup> Detection in Environmental Pollutants

Jiawei Tu<sup>1</sup>, Ying Gan<sup>1</sup>, Tao Liang<sup>1</sup>, Qiongwen Hu<sup>1</sup>, Qian Wang<sup>2</sup>, Tianling Ren<sup>2</sup>, Qiyong Sun<sup>3,4</sup>, Hao Wan<sup>1\*</sup> and Ping Wang<sup>1\*</sup>

<sup>1</sup> Biosensor National Special Laboratory, Key Laboratory for Biomedical Engineering of Ministry of Education, Department of Biomedical Engineering, Zhejiang University, Hangzhou, China, <sup>2</sup> Tsinghua National Laboratory for Information Science and Technology, Tsinghua University, Beijing, China, <sup>3</sup> Key Laboratory of Healthy & Intelligent Kitchen System Integration of Zhejiang Province, Ningbo, China, <sup>4</sup> Ningbo Fotile Kitchenware CO. LTD., Bodi Centre, Hangzhou, China

## OPEN ACCESS

### Edited by:

Larisa Lvova,  
Università degli Studi di Roma Tor  
Vergata, Italy

### Reviewed by:

Florence Lagarde,  
Claude Bernard University Lyon 1,  
France

Ajeet Kaushik,  
Florida International University,  
United States

### \*Correspondence:

Hao Wan  
wh1816@zju.edu.cn  
Ping Wang  
cnpwang@zju.edu.cn

### Specialty section:

This article was submitted to  
Analytical Chemistry,  
a section of the journal  
Frontiers in Chemistry

Received: 19 March 2018

Accepted: 17 July 2018

Published: 14 August 2018

### Citation:

Tu J, Gan Y, Liang T, Hu Q, Wang Q,  
Ren T, Sun Q, Wan H and Wang P  
(2018) Graphene FET Array Biosensor  
Based on ssDNA Aptamer for  
Ultrasensitive Hg<sup>2+</sup> Detection in  
Environmental Pollutants.  
Front. Chem. 6:333.  
doi: 10.3389/fchem.2018.00333

Invisible mercury ion is an extremely poisonous environmental pollutant, therefore, a fast and highly sensitive detection method is of significant importance. In this study, a liquid-gated graphene field-effect transistor (GFET) array biosensor (6 × 6 GFETs on the chip) was fabricated and applied for Hg<sup>2+</sup> quantitate detection based on single-stranded DNA (ssDNA) aptamer. The biosensor showed outstanding selectivity to Hg<sup>2+</sup> in mixed solutions containing various metal ions. Moreover, the sensing capability of the biosensor was demonstrated by real-time responses and showed a fairly low detection limit of 40 pM, a wide detection ranged from 100 pM to 100 nM and rapid response time below one second. These results suggest that the GFET array biosensor based on ssDNA aptamer offers a simple fabrication procedure and quite fast method for mercury ion contaminant detection and are promising for various analytical applications.

**Keywords:** biosensor, graphene FET array, Hg<sup>2+</sup> detection, ssDNA aptamer, ultrasensitive detection

## INTRODUCTION

Graphene is a two-dimensional and one-atom thick sheet of sp<sup>2</sup> hybridized carbon with exceptional electrical and physical properties, such as large detection area, ultra-high electron mobility, tunable ambipolar field-effect characteristic, and biocompatibility, compared to ones based on conventional semiconductor materials. In consequence, graphene field-effect transistor (GFET) have recently attracted much interest in sensing field (Dan et al., 2009; He et al., 2010, 2012; Huang et al., 2010, 2011; Myung et al., 2011; Kim et al., 2015; Han et al., 2017; Li et al., 2017; Kotlowski et al., 2018; Mansouri Majd and Salimi, 2018; Xu et al., 2018) for detection of DNA, protein, ions and so on. Since the first demonstrations, much progress has been achieved in the fabrication and performance of GFETs. In the sensing field, DNA aptamers combining with electrolyte-gated GFET sensor are a preferable choice, since they are smaller in size than Debye length (Maehashi et al., 2007). Therefore, the binding event between the aptamers and the targets can occur within the electric double layer in buffer solution, and as a consequence, changes in the charge distribution with proximity to the graphene can easily be detected (Guo et al., 2005; So et al., 2005). Moreover, the density of the immobilized DNA on the graphene can be controlled, and a high density of DNA can easily be prepared.

Mercury ions ( $\text{Hg}^{2+}$ ) are extremely toxic environmental pollutants, which would affect the immune and nervous systems, alter genetic expression, and cause serious damage to both mammals' health and the environment even at very low concentrations (Clarkson et al., 2003). Thus, a fast and highly sensitive  $\text{Hg}^{2+}$  detection method is of great importance in the healthcare and environmental fields. Several methods have been developed for mercury sensing, including photoelectrochemical methods (Ha et al., 2011), colorimetric analysis (Kim et al., 2012), and oligonucleotide-based sensing (Ono and Togashi, 2004). Therein, biosensing offers considerable advantages including fast response, requirement of low cost, simple equipment, and high sensitivity and selectivity. Recently, much attention has been extended to the development of optical and electrochemical techniques based on DNA for the selective  $\text{Hg}^{2+}$  detection. For example, Liu et al. (2009) developed a novel sensor for  $\text{Hg}^{2+}$  detection based on a conformational switch using ferrocene-tagged poly-thymine oligonucleotide to form thymine- $\text{Hg}^{2+}$ -thymine (T- $\text{Hg}^{2+}$ -T). A report by Zhuang et al. (2013) presented an  $\text{Hg}^{2+}$  electrochemical biosensor, which used DNA hairpins as recognition elements and exhibited a detection limit of 2.5 nM. Electrochemical strategies for mercury detection based on T- $\text{Hg}^{2+}$ -T coordination chemistry have been reported by Wang et al. (2014).

At present, the studies of GFET were basically based on a single sensor (Ohno et al., 2009; An et al., 2013; Mansouri Majd and Salimi, 2018), but single GFET has a low current that increases the difficulty of circuit design and signal acquisition. Further, due to the variation of graphene and individual FET, consistent results are hard to be obtained with a single sensor. Therefore, in this study, a common-source array design was used to obtain a large current response and reduce the impact of individual differences. To the best of our knowledge, no study based on GFET array was reported for  $\text{Hg}^{2+}$  detection with the modification of ssDNA.

Herein, a novel biosensor for  $\text{Hg}^{2+}$  ultrasensitive determination was designed and fabricated based on common-source graphene field-effect transistors array ( $6 \times 6$  GFETs) and ssDNA aptamer. The performance of biosensor was explored by analyzing the Raman spectrum, electrical properties, interferences, and so on. Furthermore, the GFET array modified by ssDNA sequences was applied to  $\text{Hg}^{2+}$  quantitative determination, which provided a promising method for fast and highly sensitive detection of  $\text{Hg}^{2+}$  in a variety of applications.

## METHODS

### System and Materials

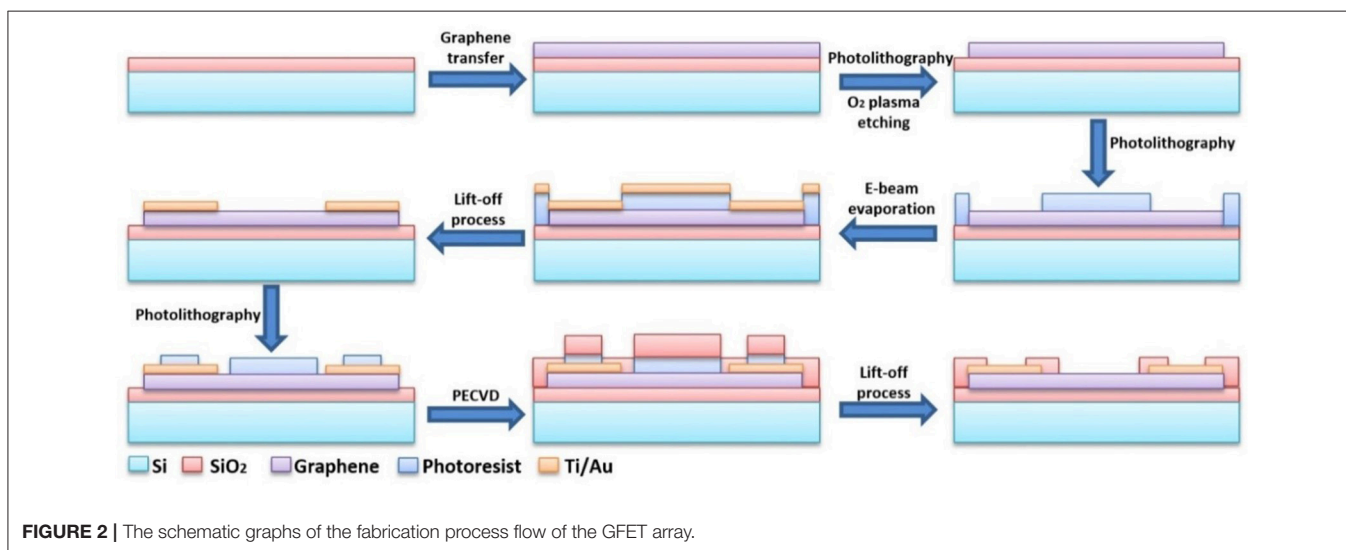
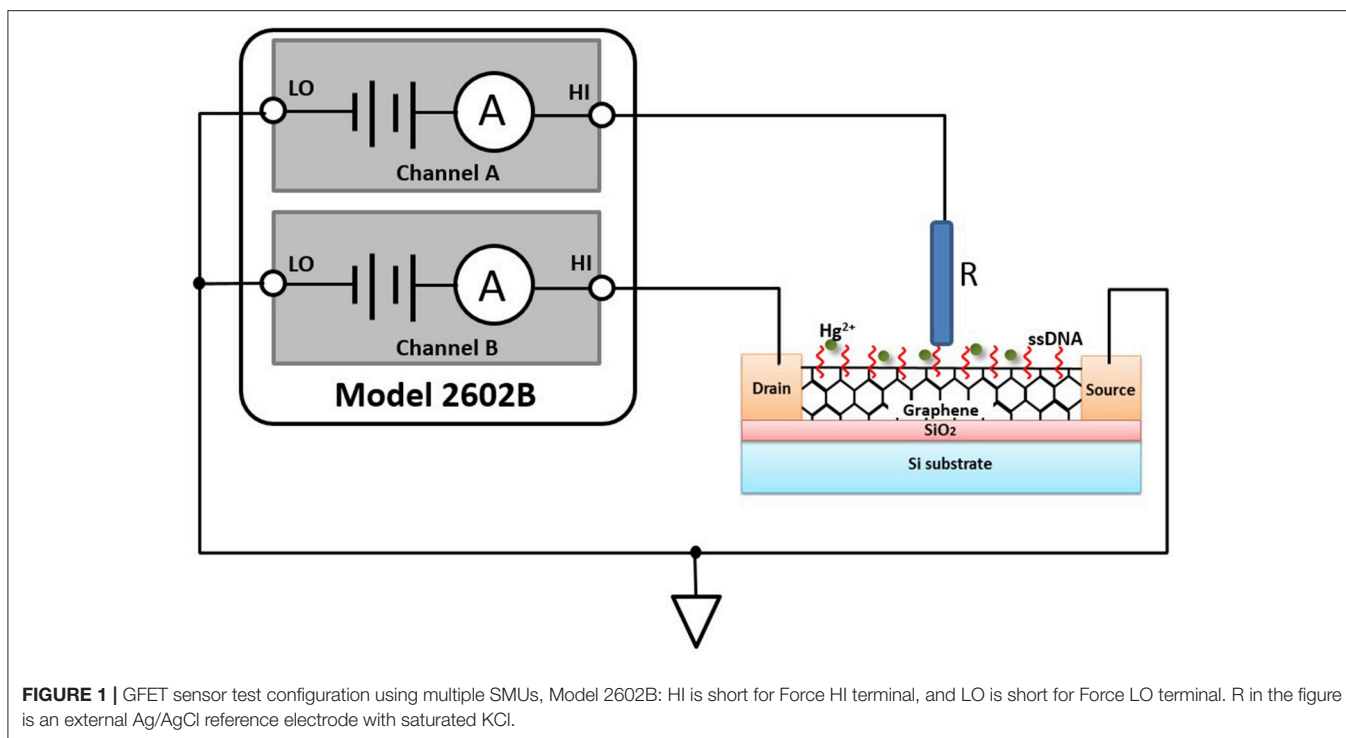
Characterizing GFET array's current-voltage (I-V) parameters is extremely crucial to ensuring that it works properly as a sensor and meets specifications. In general, FET-type sensor characteristics testing involves the use of several kinds of instruments, including a sensitive ammeter, multiple voltage sources, and a voltmeter or an alternative approach, a turnkey semiconductor characterization system, which are either tedious or expensive. In our study, Model 2602B (Keithley Instruments Inc., USA), a two-channel source measurement unit (SMU), was utilized to perform parameter testing on the GFET array sensor.

The Model 2602B has current resolution to 0.1 fA and can be current limited to prevent damage to the sensor. **Figure 1** illustrated an I-V test configuration for an electrolyte-gated GFET sensor using a two-channel Model 2602B, and the GFET sensor had three main terminals: the electrolyte gate, the drain, and the source. A voltage applied to the gate terminal ( $V_G$ ) controlled the resulting drain current ( $I_{DS}$ ) that flowed from the drain to the source terminal. In this configuration, the Force HI terminal of Channel A was connected to the gate of the sensor and the Force HI terminal of Channel B was connected to the drain. And the source terminal of the sensor was connected to the Force LO terminals of both SMU channels. A common I-V test performed on the sensor was the drain family of curves ( $V_G$ - $I_{DS}$ ). With this test, SMU CHB stepped the drain voltage ( $V_{DS}$ ) with a step of 0.1 V from 0 to 3.0 V while SMU CHA swept the gate voltage ( $V_G$ ) from -4.0 to 4.0 V and measured the resulting drain current. An external Ag/AgCl reference electrode (saturated KCl) worked as the electrolyte gate of the sensor, which was connected to the Force HI terminal of Channel A.

Reagents used in the experiment were all of analytical grade. Deionized water ( $18.4 \text{ M}\Omega \cdot \text{cm}$ ) used for cleaning and dilution was prepared by an ultra-pure water system Mili-Q (Millipore, USA). The mercury standard solution ( $100 \mu\text{g}/\text{mL}$  in 3%  $\text{HNO}_3$ ) was purchased from the National Research Center for Certified Reference Material, China, and de-ionized water was used to dilute the standard solution into different concentrations. Other reagents were purchased from Aladdin (Shanghai, China) and used as received. Analytical grade copper chloride, lead nitrate, chromium chloride, and cadmium chloride were used to prepare stock solutions of 1,000 mg/L of the four metal ions, which were further diluted to the required concentrations before use. The ssDNA was custom-synthesized by GenScript Corp. (USA) and purified by high-performance liquid chromatography. The anti- $\text{Hg}^{2+}$  ssDNA sequence used in this study was as follows: 5'-GTTCTTTTCGGCTTTGTTC-3'-C7-amino, which could easily form the T- $\text{Hg}^{2+}$ -T configuration in the presence of  $\text{Hg}^{2+}$  (Lee et al., 2007; Li et al., 2008). All experiments were carried out at room temperature.

### GFET Array Fabrication

The schematic graphs of the detailed fabrication process flow of the GFET array was shown in **Figure 2**. The GFET array was fabricated with a series of photolithography methodologies. The graphene film used in the sensor was synthesized by chemical vapor deposition (CVD) on a copper foil and transferred to highly doped silicon substrate with 90 nm thick thermally grown  $\text{SiO}_2$  capping layer. After being spin-coated with polymethylmethacrylate (PMMA), the graphene/Cu film was placed on the surface of the etching solution (1 M  $\text{FeCl}_3$  and 1 M HCl) until the copper foil was completely etched away. And then, the graphene/PMMA film was rinsed by deionized water for several times before transferred onto substrates. PMMA was subsequently removed by acetone. After graphene being transferred, standard photolithography was employed to pattern the channel region of graphene and oxygen plasma etching to remove the unwanted graphene. Next, the metallic layer, which included a titanium layer of 20 nm and a gold layer of 50 nm, was sputtered by e-beam evaporation on the substrate, in which the



titanium layer acted as the adhesion layer. And, photolithography was utilized once again to define the shapes of source and drain electrodes followed by lift-off process. Afterwards, a SiO<sub>2</sub> layer of 100 nm was deposited with plasma enhanced chemical vapor deposition (PECVD) on the metallic layer for insulation. Ultimately, partial insulation areas were etched to expose a designated gold area for spot welding to the external bonding pad and a designed graphene area as the electrolyte gate for the GFET sensor. The final structure of GFET array was seen at the lower right in **Figure 2**.

The GFET array was manufactured after all the fabrications mentioned above, the size of which was 9.2 × 9.2 mm.

As shown in the **Figure 3a**, the whole packaged chip of GFET array with printed circuit board (PCB) was 4.2 × 4.2 cm, consisted of 6 × 6 common-source GFETs, with the exposed area of 60 × 80 μm each GFET separated by an 800 μm gap. According to the technical processes above, the graphene was exposed as the electrolyte gate for GFET, just as the blue parts in **Figures 3b,c**, while the source and drain electrodes (the gold parts in **Figures 3b,c**) were covered by 100 nm SiO<sub>2</sub> as the insulating layer. **Figure 3b** showed that the 36 GFETs ranked neatly in parallel, which meant all the 36 GFETs shared one source electrode. Finally, the bonding pads of GFET array chip were connected to

PCB pads by gold wires and a cell was used in chip encapsulation.

### Fabrication of Biosensor

To utilize the GFET array as an ultra-sensitive sensor for  $\text{Hg}^{2+}$  detection, DNA aptamer with plentiful thymine was functionally attached to the graphene film surface to selectively determine

the  $\text{Hg}^{2+}$ . According to the literatures (Chen et al., 2001; Kwon et al., 2012; Park et al., 2012; An et al., 2013), one of the most efficient condensing agents, 1,5-diaminonaphthalene (DAN), was stacked on the side plane of the graphene by  $\pi$ - $\pi$  interactions between the naphthalene group of DAN and its  $\text{sp}^2$ -carbon plane. Hence, the GFET array was treated with  $10 \mu\text{M}$  DAN in methanol ( $40 \mu\text{L}$ ) for 3 h at room temperature and then flushed with

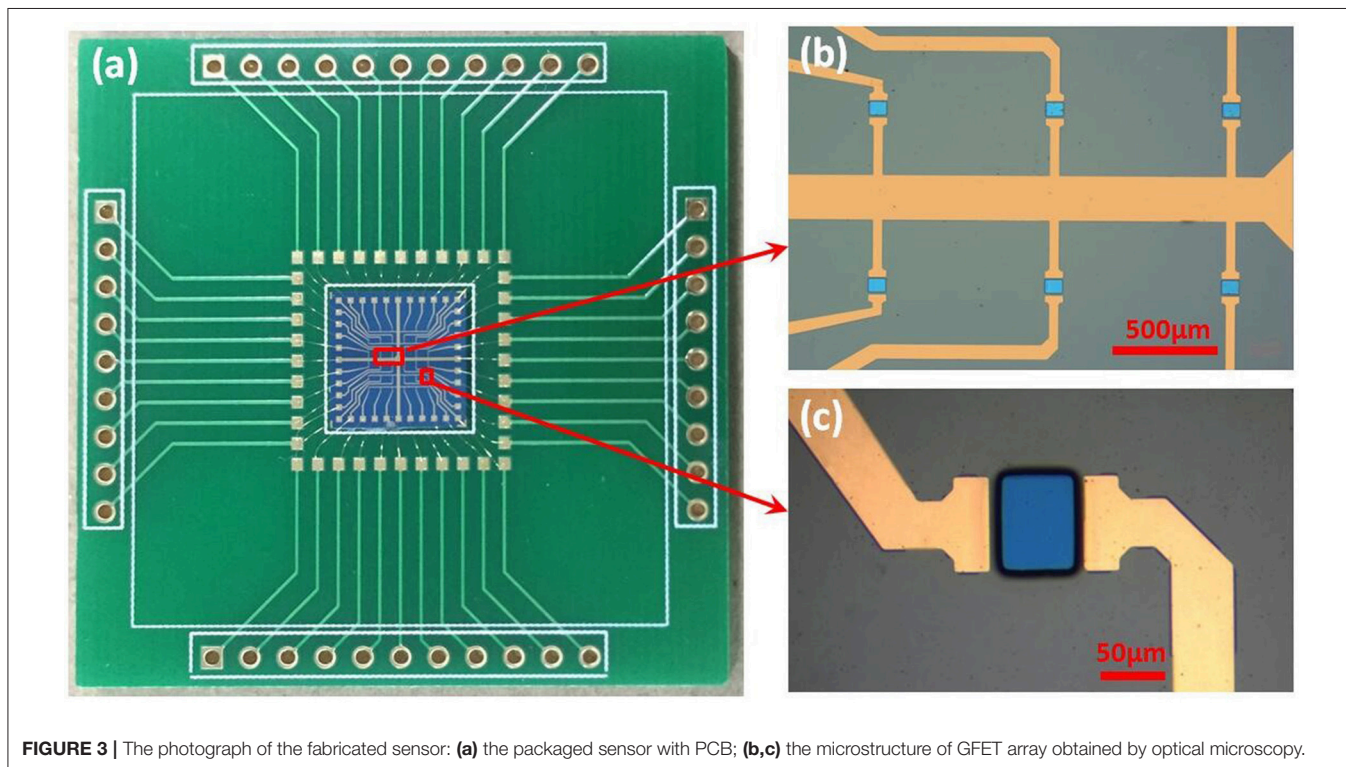


**FIGURE 3** | The photograph of the fabricated sensor: (a) the packaged sensor with PCB; (b,c) the microstructure of GFET array obtained by optical microscopy.

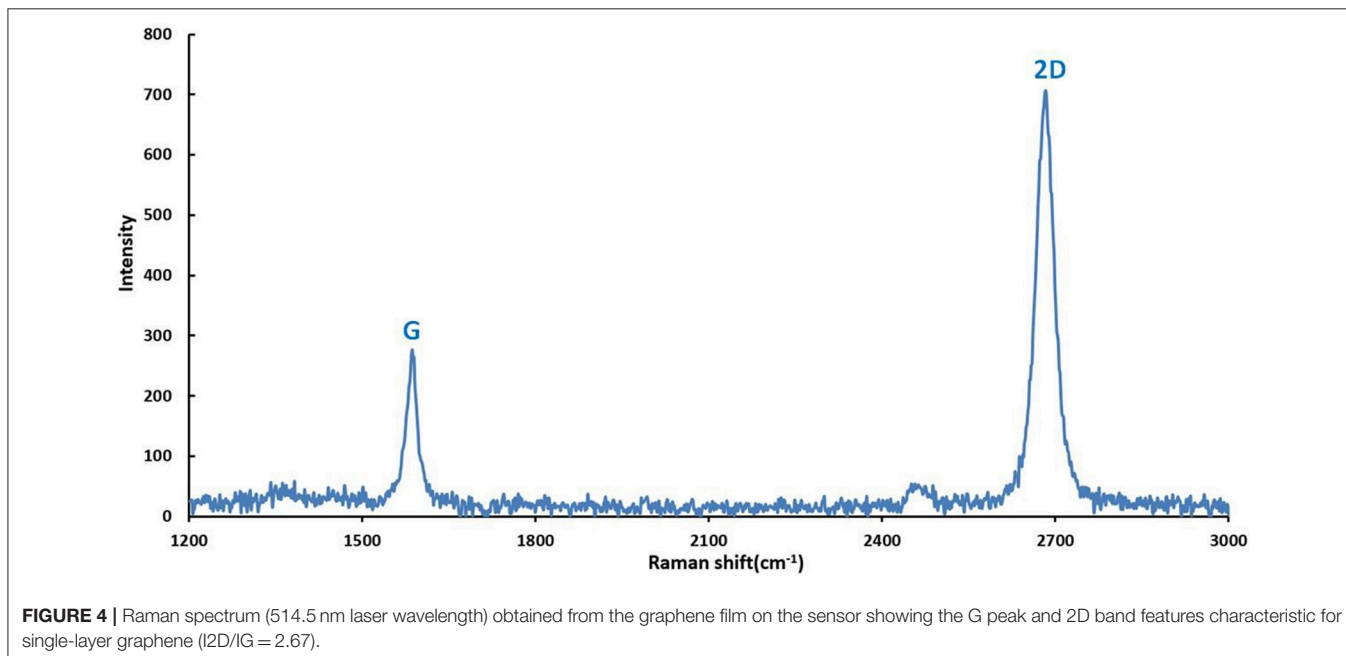


**FIGURE 4** | Raman spectrum (514.5 nm laser wavelength) obtained from the graphene film on the sensor showing the G peak and 2D band features characteristic for single-layer graphene ( $I_{2D}/I_G = 2.67$ ).

0.01 M phosphate buffer solution (PBS, pH 7.4). After that, 40  $\mu\text{L}$  2% (v/v) glutaraldehyde (GA) was conjugated DAN through a Schiff-base reaction in pure environments for another 3 h. The Schiff-base reaction proceeded through chemical attachment between the aldehyde group of GA and the amine group of the DAN connected at the graphene (Lee et al., 2006). Subsequently, after flushing the chip with PBS to remove the superfluous GA, 40  $\mu\text{L}$  ssDNA (20  $\mu\text{M}$  in 0.01 M Tris-HCl buffer solution, pH 7.4) was immobilized to the GA on the graphene surface over 6 h at room temperature, which was also based on the Schiff-base reaction. Finally, the desired ssDNA-based biosensor for  $\text{Hg}^{2+}$  specific detection was fabricated and rinsed with surplus PBS.

## RESULTS AND DISCUSSION

### Characterization of Common-Source Liquid-Gated GFET Array

#### Characterization of Graphene on the GFET

According to the methods for graphene fabrication described in part 2.2 of this study, graphene film was synthesized by CVD on copper foils and patterned with proper shape after being transferred onto Si/SiO<sub>2</sub> substrates. Subsequently, the properties of graphene on the surface of GFET array were explored by Raman spectra analysis. The **Figure 4** illustrated the Raman spectrum obtained from the graphene film on the GFET array sensor at 514.5 nm laser excitation. The graphene film exhibited typical monolayer graphene features with a sharp G peak and a single 2D peak with a higher intensity. The two prominent peaks appeared at approximate 1,589 and 2,683  $\text{cm}^{-1}$ , corresponding to G and 2D peaks, respectively. And, the peak intensity ratio of 2.67 between 2D and G confirmed the high percentage of monolayer with fewer multilayer islands in the graphene film on the sensor (Ferrari et al., 2006; Park et al., 2011; Zang et al., 2011; Tian et al., 2012). Meanwhile, the absence of D-band in this spectrum also confirmed the high quality of the as-grown graphene with fewer defects (Graf et al., 2007; Li et al., 2009; Tian et al., 2011).

#### Characterization of Common-Source GFET Array

The signal superposition characteristics of the common-source GFET array was shown in **Figure 5**. The curves in the lower part of **Figure 5** showed the characteristics of six independent GFETs. The red curve in the upper part of **Figure 5** was the signal summation of the six independent GFETs. After connecting these six GFETs in parallel, the characteristic curve was shown as the blue curve. It can be seen that the signal intensity of the common-source GFETs had been significantly enhanced compared to a single sensor. The amplitude of superimposed current was the same as the current amplitude in the parallel condition, but the potential shifted because the reference electrode position changed. With the same reason, different single GFET had different distances from the reference electrode, so the characteristic curves of the six independent GFETs were also different. Therefore, in order to increase the response current, the array structure was effective.

### Characterization of Liquid-Gated GFET Array

For the capability test of GFET array, the electrical properties of the liquid-gated GFET array were investigated in the 0.01 M PBS (pH 7.4) at room temperature. The electrical measurements were conducted by the multiple SMUs system described above. The **Figure 6** showed that gate voltage ( $V_G$ ) was swept from  $-0.8$  to  $2.0$  V and the resulting drain current was measured at a gradient changing drain voltage ( $V_{DS}$ ) with a step of  $0.1$  V from  $0$  to  $0.8$  V. With increasing gate bias using the reference electrode, the source-drain current decreased in the beginning ( $V_G < 0.8$  V), and then increased, which indicated

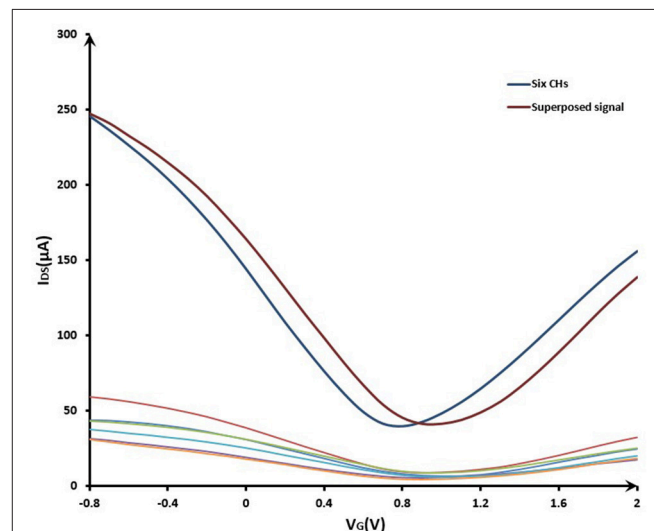


**FIGURE 5** | The signal superposition characteristics of the common-source GFET array.  $V_G$  sweeping from  $-0.8$  to  $2.0$  V;  $V_{DS} = 0.5$  V.

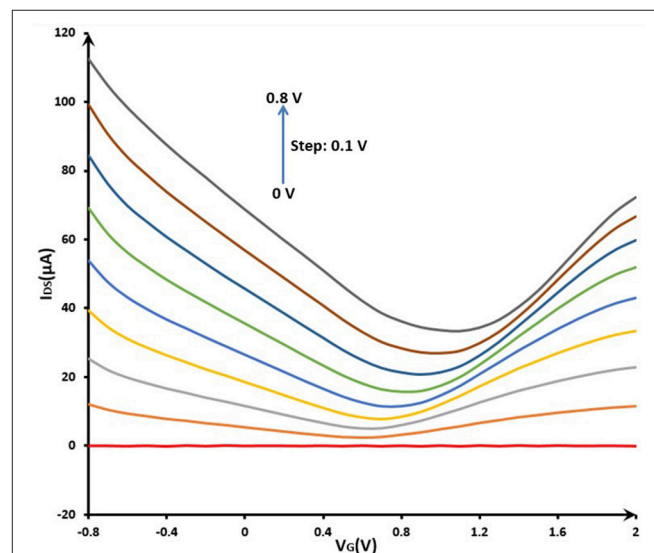


**FIGURE 6** | Electrical properties ( $I_{DS}$ - $V_G$  curve) of GFET array device before modification in phosphate buffer solution (0.01 M PBS, pH 7.4):  $V_G$  sweeping from  $-0.8$  to  $2.0$  V;  $V_{DS}$  changing from  $0$  to  $0.8$  V with a step of  $0.1$  V.

significant bipolar characteristics in blank PBS. The  $I_{DS}$ - $V_G$  curve of GFET array device showed a remarkable Dirac point, which illustrated the structural integrity of common-source graphene FET array sensor. Meanwhile, a suitable quiescent bias point should be considered very cautiously in order

to obtain a high dynamic range and steady response for the sensor application. In this way, according to the  $I_{DS}$ - $V_G$  curves, this point was expected to be located around  $V_{DS} = 0.4\sim 0.8\text{ V}$  and  $V_G = -0.8\sim -0.4\text{ V}$  for the present device.

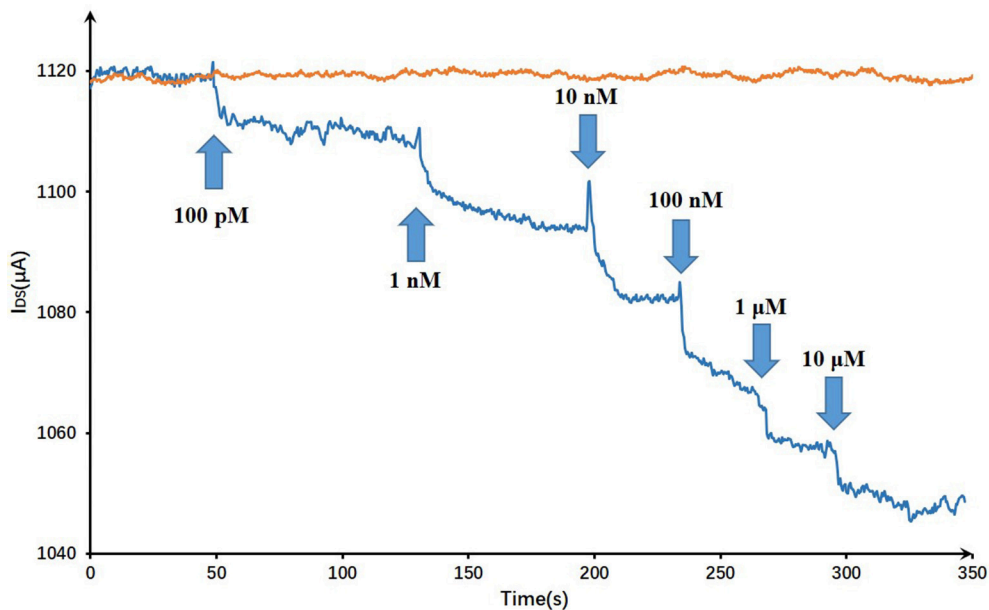


**FIGURE 7** | Dynamic responses of the DNA-based biosensor to  $\text{Hg}^{2+}$  and a blank control: the arrows pointed the adding time and corresponding concentrations.

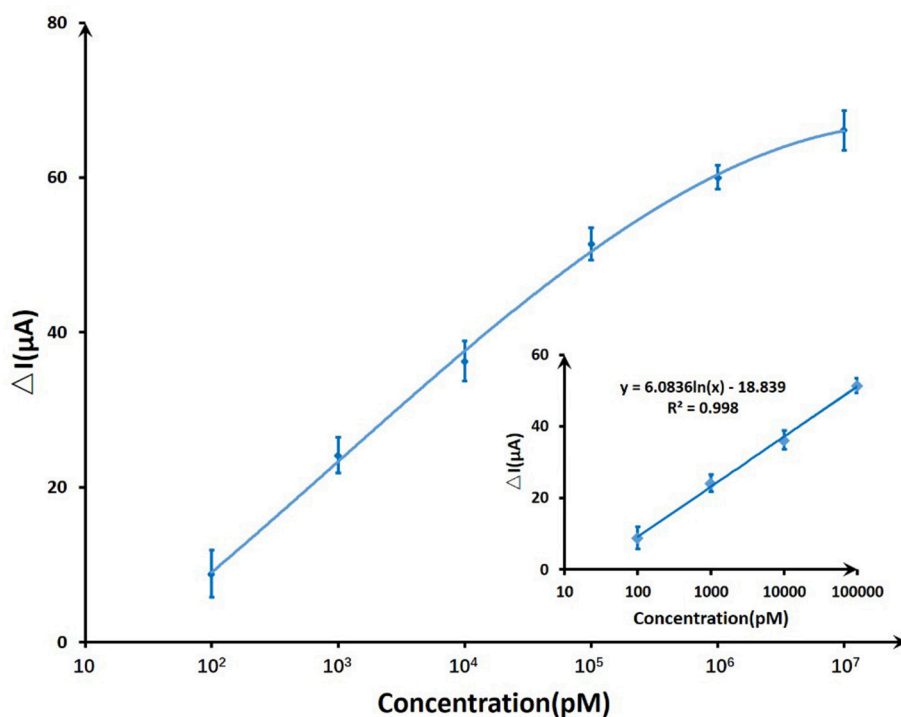


**FIGURE 8** | The sensitivity trendline of DNA-based GFET array biosensor to mercury ions ranging from 100 pM to 10  $\mu\text{M}$ . A linear fit was given for the first four concentrations.

## Analytical Figures of Merit of the GFET Biosensor Array

On account of T-Hg<sup>2+</sup>-T reaction, Hg<sup>2+</sup> ions binding to the ssDNA aptamer results electrostatic change at the interface, which will induce a change in the electrical signals. The biosensor performance was demonstrated by measuring I<sub>DS</sub> upon the addition of various mercury concentrations at a constant V<sub>G</sub> (V<sub>G</sub> = -0.8 V) and V<sub>DS</sub> (V<sub>DS</sub> = 0.5 V). **Figure 7** displayed the real-time responses of GFET biosensor with ssDNA aptamer to different Hg<sup>2+</sup> concentrations, and I<sub>DS</sub> gradually decreased when exposed to higher concentrations of Hg<sup>2+</sup> within concentrations ranging from 100 pM to 10 μM. Moreover, the response time of the GFET array biosensor in the Hg<sup>2+</sup> determination was pretty fast (on a time scale of <1 s). The biosensor showed a concentration-dependent decrease in I<sub>DS</sub> when it was exposed to the target Hg<sup>2+</sup>, and in order to further characterize the sensitivity of the ssDNA-based biosensor, the correlation between drain-source current and the logarithm of Hg<sup>2+</sup> concentration [ln(con)] was investigated as shown in **Figure 8**. The standard deviations (SDs) in all concentrations were calculated ranging from ±1.54 to ±3.02 μA, and the largest relative standard deviation (RSD) in all concentrations is 9.1%. This low RSD indicates very good repeatability of this biosensor for mercury detection. The current variation increased from 100 pM to 10 μM of the Hg<sup>2+</sup> concentration. The saturation of the sensor was observed over 1 μM, so the biosensor was calibrated based the

current variation of the first four samples. According to the fitting results, the correlation index ( $R^2$ ) between I<sub>DS</sub> and ln(con) was 0.998, which showed a quite high correlation between them. Furthermore, the GFET biosensor array exhibited a detection limit of about 40 pM (RSD = 48.64%), which could meet the requirements for Hg<sup>2+</sup> applications.

The purpose of the experiments wanted to investigate the interference factors for the Hg<sup>2+</sup> measurements. To evaluate the selectivity of the sensing system for Hg<sup>2+</sup> ion, the responses of the ssDNA-based biosensor to various suspicious interfering metal ions, which were added in blank 0.01 M PBS (pH 7.4) as analytical samples, were recorded. As **Figure 9** showed, Cu<sup>2+</sup>, Pb<sup>2+</sup>, Cr<sup>3+</sup>, Cd<sup>2+</sup> of 10 nM and Hg<sup>2+</sup> of 100 pM were added successively in 0.01 M PBS, and the selective responses of GFET array biosensor were recorded for 200 s. From 0 to 160 s, the responses had no obvious change until the addition of Hg<sup>2+</sup> even in the case that the concentrations of competing ions were a hundred times greater than Hg ion. 100 pM Hg<sup>2+</sup> could induce a significant current reduction of the biosensor, indicating that the biosensor exhibits a high selectivity to Hg<sup>2+</sup> over other competing ones.

## Comparison

Compared to other methods and sensors for Hg<sup>2+</sup> detection, this GFET biosensor array presents high performance (**Table 1**). The first two studies are based on FET to detect Hg<sup>2+</sup>, and the third study used electrochemical impedance spectroscopy

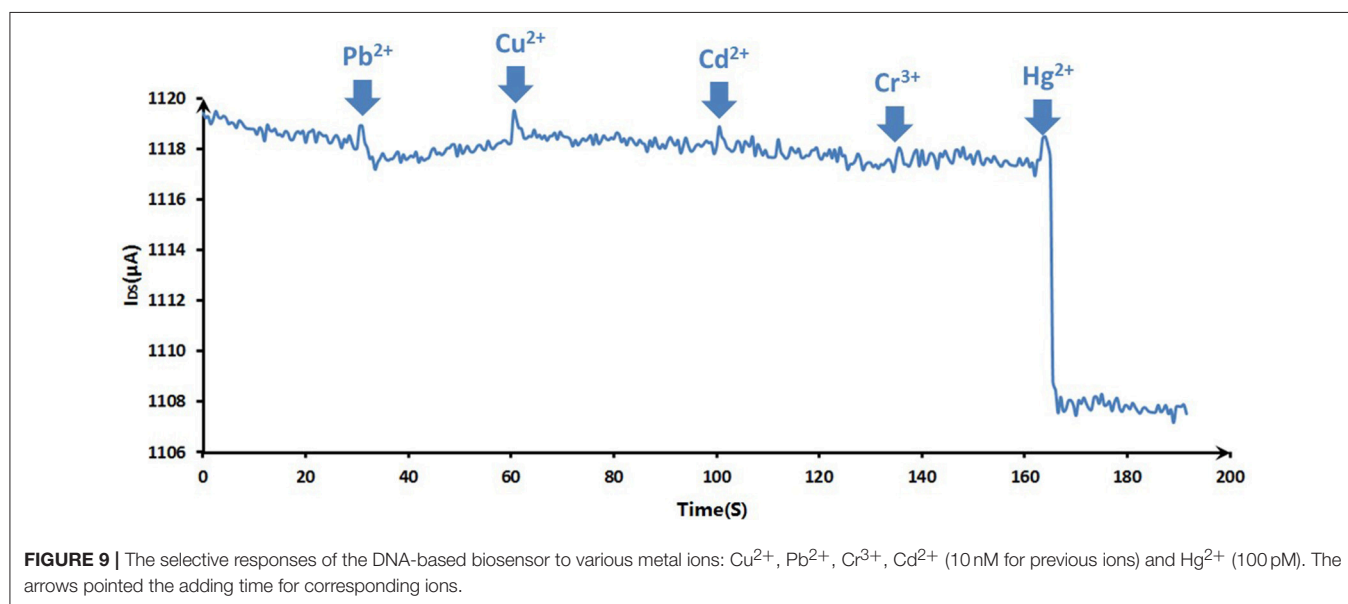


**FIGURE 9** | The selective responses of the DNA-based biosensor to various metal ions: Cu<sup>2+</sup>, Pb<sup>2+</sup>, Cr<sup>3+</sup>, Cd<sup>2+</sup> (10 nM for previous ions) and Hg<sup>2+</sup> (100 pM). The arrows pointed the adding time for corresponding ions.

**TABLE 1** | Comparison of Hg<sup>2+</sup> detection methods and sensors.

Detection method	Sensor	Detection range	Detection limit	References
Gate voltage	Alkanethiol modified GFET	Not mentioned	10 ppm (50 nM)	Zhang et al., 2010
Gate voltage	MoS <sub>2</sub> /DNA-Au NPs FET	0.1–10 nM	0.1 nM	Zhou et al., 2016
EIS	Gold disk electrode	0.1 nM–10 μM	0.1 nM	Lin et al., 2011
Electrochemical	Au microelectrode array	10–100 nM	4 nM	Huan et al., 2012
Gate voltage	ssDNA aptamer GFET array	0.1–100 nM	40 pM	This work

(EIS) measurement based on the T-Hg<sup>2+</sup>-T principle. The fourth work used electrochemical detection for Hg<sup>2+</sup> based on Au microelectrode array. Compared to other sensors, this ssDNA aptamer GFET array presents wider detection range from 0.1 to 100 nM and the lowest detection limit of 40 pM.

Due to the very tight bonding between T-Hg<sup>2+</sup>-T, the current response would keep decreasing when bonding with more Hg<sup>2+</sup>. Thus, the response baseline would keep changing during the stability test, which is hard to be evaluated. The biosensor can be recycled before the saturation of the biosensor. Between the two measurements, the biosensor should be kept in 4°C to maintain the performance of the biosensor. When starting the measurement, the biosensor should be washed using PBS and measured in a blank sample to obtain a stable baseline. Then the biosensor can be used for the following tests.

For detecting Hg<sup>2+</sup>, the GFET array is highly sensitive, and capable for online and continuous monitoring. However, unlike detection in a buffer, water contaminant detection is usually carried out in a natural water system. In natural environment, mercury may exist as complexes which can have an effect on the results. Moreover, the suspended solid and organic and inorganic materials in water may disturb the GFET signal, leading to large uncertainties during the detection and may reduce the sensitivity and lifetime of the sensor. Therefore, to extend the GFET array into practical applications, further work is needed.

## CONCLUSION

A liquid-gated GFET array with 36 common-source FETs was fabricated and applied for Hg<sup>2+</sup> detection as a biosensor decorated with ssDNA aptamer. The characterization of GFET

array was tested and discussed based on the Raman spectrum and electrical methods on the multiple SMUs system. The array structure with common-source was effective in increasing the response current. The biosensor showed good selectivity to Hg<sup>2+</sup> in mixed solutions containing various metal ions. Moreover, the sensing capability of the biosensor was demonstrated by real-time responses and showed a fairly low detection limit of about 40 pM and quite rapid response time below 1 s. Compared with other similar detection methods and sensors, the constructed biosensor presents an excellent detection level. Overall, the simple fabrication procedure and the excellent sensing performance of the GFET array structure make it promising for contaminant detection of Hg<sup>2+</sup> in water environment.

## AUTHOR CONTRIBUTIONS

JT, QS, TR, and PW conceived the idea and designed the experiments. TL, QW, and TR designed and manufactured sensors. JT, YG, QH, and HW performed experiments. JT, YG, TL, QW, QH, and HW contributed to data analysis and interpretation. JT and PW wrote this paper. All authors discussed the results and commented on the manuscript.

## FUNDING

Financial support provided by Ministry of Science and Technology of China (973 Program) (Grant No. 2015CB352101), Natural Science Foundation of NSFCRFB Cooperation of China (Grant No. 8171101322) and Major Research and Development Program of Zhejiang Province (Grant No. 2017C03032), is gratefully acknowledged.

## REFERENCES

- An, J. H., Park, S. J., Kwon, O. S., Bae, J., and Jang, J. (2013). High-performance flexible graphene aptasensor for mercury detection in mussels. *ACS Nano* 7, 10563–10571. doi: 10.1021/nn402702w
- Chen, R. J., Zhang, Y., Wang, D., and Dai, H. (2001). Noncovalent sidewall functionalization of single-walled carbon nanotubes for protein immobilization. *J. Am. Chem. Soc.* 123, 3838–3839. doi: 10.1021/ja010172b
- Clarkson, T. W., Magos, L., and Myers, G. J. (2003). The toxicology of mercury—current exposures and clinical manifestations. *N. Engl. J. Med.* 349, 1731–1737. doi: 10.1056/NEJMra022471
- Dan, Y., Lu, Y., Kybert, N. J., Luo, Z., and Johnson, A. T. (2009). Intrinsic response of graphene vapor sensors. *Nano Lett.* 9, 1472–1475. doi: 10.1021/nl8033637
- Ferrari, A. C., Meyer, J., Scardaci, V., Casiraghi, C., Lazzeri, M., Mauri, F., et al. (2006). Raman spectrum of graphene and graphene layers. *Phys. Rev. Lett.* 97:187401. doi: 10.1103/PhysRevLett.97.187401
- Graf, D., Molitor, F., Ensslin, K., Stampfer, C., Jungens, A., Hierold, C., et al. (2007). Spatially resolved Raman spectroscopy of single- and few-layer graphene. *Nano Lett.* 7, 238–242. doi: 10.1021/nl061702a
- Guo, X., Huang, L., O'Brien, S., Kim, P., and Nuckolls, C. (2005). Directing and sensing changes in molecular conformation on individual carbon nanotube field effect transistors. *J. Am. Chem. Soc.* 127, 15045–15047. doi: 10.1021/ja054335y
- Ha, D., Yu, H., Hu, N., Wu, C., Zhou, J., Kirsanov, D., et al. (2011). “Portable e-tongue based on multi-channel LAPS array with PVC membrane for rapid environment detection,” in *AIP Conference Proceedings*, AIP (New York, NY), 187–188.
- Han, D., Chand, R., and Kim, Y. S. (2017). Microscale loop-mediated isothermal amplification of viral DNA with real-time monitoring on solution-gated graphene FET microchip. *Biosens. Bioelectron.* 93, 220–225. doi: 10.1016/j.bios.2016.08.115
- He, Q., Sudibya, H. G., Yin, Z., Wu, S., Li, H., Boey, F., et al. (2010). Centimeter-long and large-scale micropatterns of reduced graphene oxide films: fabrication and sensing applications. *ACS Nano* 4, 3201–3208. doi: 10.1021/nn100780v
- He, Q., Wu, S., Yin, Z., and Zhang, H. (2012). Graphene-based electronic sensors. *Chem. Sci.* 3, 1764–1772. doi: 10.1039/c2sc20205k
- Huan, T. N., Hung, L. Q., Ha, V. T., Anh, N. H., Van Khai, T., and Chung, H. (2012). Spirally oriented Au microelectrode array sensor for detection of Hg (II). *Talanta* 94, 284–288. doi: 10.1016/j.talanta.2012.03.041
- Huang, Y., Dong, X., Liu, Y., Li, L.-J., and Chen, P. (2011). Graphene-based biosensors for detection of bacteria and their metabolic activities. *J. Mater. Chem.* 21, 12358–12362. doi: 10.1039/c1jm11436k
- Huang, Y., Dong, X., Shi, Y., Li, C. M., Li, L. J., and Chen, P. (2010). Nanoelectronic biosensors based on CVD grown graphene. *Nanoscale* 2, 1485–1488. doi: 10.1039/c0nr00142b
- Kim, H. N., Ren, W. X., Kim, J. S., and Yoon, J. (2012). Fluorescent and colorimetric sensors for detection of lead, cadmium, and mercury ions. *Chem. Soc. Rev.* 41, 3210–3244. doi: 10.1039/C1CS15245A
- Kim, J., Lee, M. S., Jeon, S., Kim, M., Kim, S., Kim, K., et al. (2015). Highly transparent and stretchable field-effect transistor sensors using graphene-nanowire hybrid nanostructures. *Adv. Mater.* 27, 3292–3297. doi: 10.1002/adma.201500710



- Kotlowski, C., Larisika, M., Guerin, P. M., Kleber, C., Kröber, T., Mastrogiacomo, R., et al. (2018). Fine discrimination of volatile compounds by graphene-immobilized odorant-binding proteins. *Sens. Actuat. B* 256, 564–572. doi: 10.1016/j.snb.2017.10.093
- Kwon, O. S., Park, S. J., Hong, J. Y., Han, A. R., Lee, J. S., and Jang, J. (2012). Flexible FET-type VEGF aptasensor based on nitrogen-doped graphene converted from conducting polymer. *ACS Nano* 6, 1486–1493. doi: 10.1021/nn204395n
- Lee, J. S., Han, M. S., and Mirkin, C. A. (2007). Colorimetric detection of mercuric ion (Hg<sup>2+</sup>) in aqueous media using DNA-functionalized gold nanoparticles. *Angew. Chem.* 119, 4171–4174. doi: 10.1002/ange.200700269
- Lee, L. M., Heimark, R. L., Baygents, J. C., and Zohar, Y. (2006). Self-aligned immobilization of proteins utilizing PEG patterns. *Nanotechnology* 17:S29. doi: 10.1088/0957-4484/17/4/006
- Li, D., Wieckowska, A., and Willner, I. (2008). Optical analysis of Hg<sup>2+</sup> ions by oligonucleotide-gold-nanoparticle hybrids and DNA-based machines. *Angew. Chem.* 120, 3991–3995. doi: 10.1002/ange.200705991
- Li, X., Cai, W., An, J., Kim, S., Nah, J., Yang, D., et al. (2009). Large-area synthesis of high-quality and uniform graphene films on copper foils. *Science* 324, 1312–1314. doi: 10.1126/science.1171245
- Li, Y., Wang, C., Zhu, Y., Zhou, X., Xiang, Y., He, M., et al. (2017). Fully integrated graphene electronic biosensor for label-free detection of lead (II) ion based on G-quadruplex structure-switching. *Biosens. Bioelectron.* 89, 758–763. doi: 10.1016/j.bios.2016.10.061
- Lin, Z., Li, X., and Kraatz, H. B. (2011). Impedimetric immobilized DNA-based sensor for simultaneous detection of Pb<sup>2+</sup>, Ag<sup>+</sup>, and Hg<sup>2+</sup>. *Anal. Chem.* 83, 6896–6901. doi: 10.1021/ac2014096
- Liu, S. J., Nie, H. G., Jiang, J. H., Shen, G. L., and Yu, R. Q. (2009). Electrochemical sensor for mercury (II) based on conformational switch mediated by interstrand cooperative coordination. *Anal. Chem.* 81, 5724–5730. doi: 10.1021/ac900527f
- Maehashi, K., Katsura, T., Kerman, K., Takamura, Y., Matsumoto, K., and Tamiya, E. (2007). Label-free protein biosensor based on aptamer-modified carbon nanotube field-effect transistors. *Anal. Chem.* 79, 782–787. doi: 10.1021/ac060830g
- Mansouri Majid, S., and Salimi, A. (2018). Ultrasensitive flexible FET-type aptasensor for CA 125 cancer marker detection based on carboxylated multiwalled carbon nanotubes immobilized onto reduced graphene oxide film. *Anal. Chim. Acta* 1000, 273–282. doi: 10.1016/j.aca.2017.11.008
- Myung, S., Solanki, A., Kim, C., Park, J., Kim, K. S., and Lee, K. B. (2011). Graphene-encapsulated nanoparticle-based biosensor for the selective detection of cancer biomarkers. *Adv. Mater.* 23, 2221–2225. doi: 10.1002/adma.201100014
- Ohno, Y., Maehashi, K., Yamashiro, Y., and Matsumoto, K. (2009). Electrolyte-gated graphene field-effect transistors for detecting pH and protein adsorption. *Nano Lett.* 9, 3318–3322. doi: 10.1021/nl901596m
- Ono, A., and Togashi, H. (2004). Highly selective oligonucleotide-based sensor for mercury (II) in aqueous solutions. *Angew. Chem. Int. Edn.* 43, 4300–4302. doi: 10.1002/anie.200454172
- Park, J., Xiong, W., Gao, Y., Qian, M., Xie, Z., Mitchell, M., et al. (2011). Fast growth of graphene patterns by laser direct writing. *Appl. Phys. Lett.* 98:123109. doi: 10.1063/1.3569720
- Park, S. J., Kwon, O. S., Lee, S. H., Song, H. S., Park, T. H., and Jang, J. (2012). Ultrasensitive flexible graphene based field-effect transistor (FET)-type bioelectronic nose. *Nano Lett.* 12, 5082–5090. doi: 10.1021/nl301714x
- So, H. M., Won, K., Kim, Y. H., Kim, B. K., Ryu, B. H., Na, P. S., et al. (2005). Single-walled carbon nanotube biosensors using aptamers as molecular recognition elements. *J. Am. Chem. Soc.* 127, 11906–11907. doi: 10.1021/ja053094r
- Tian, H., Ren, T. L., Xie, D., Wang, Y. F., Zhou, C. J., Feng, T. T., et al. (2011). Graphene-on-paper sound source devices. *ACS Nano* 5, 4878–4885. doi: 10.1021/nn2009535
- Tian, H., Xie, D., Yang, Y., Ren, T. L., Wang, Y. F., Zhou, C. J., et al. (2012). Single-layer graphene sound-emitting devices: experiments and modeling. *Nanoscale* 4, 2272–2277. doi: 10.1039/c2nr11572g
- Wang, W., Wang, Y., Tu, L., Klein, T., Feng, Y., Li, Q., et al. (2014). Magnetic detection of mercuric ion using giant magnetoresistance-based biosensing system. *Anal. Chem.* 86, 3712–3716. doi: 10.1021/ac404015j
- Xu, S., Jiang, S., Zhang, C., Yue, W., Zou, Y., Wang, G., et al. (2018). Ultrasensitive label-free detection of DNA hybridization by sapphire-based graphene field-effect transistor biosensor. *Appl. Surf. Sci.* 427, 1114–1119. doi: 10.1016/j.apsusc.2017.09.113
- Zang, Y., Xie, D., Wu, X., Chen, Y., Lin, Y., Li, M., et al. (2011). Enhanced photovoltaic properties in graphene/polycrystalline BiFeO<sub>3</sub>/Pt heterojunction structure. *Appl. Phys. Lett.* 99:132904. doi: 10.1063/1.3644134
- Zhang, T., Cheng, Z., Wang, Y., Li, Z., Wang, C., Li, Y., et al. (2010). Self-assembled 1-octadecanethiol monolayers on graphene for mercury detection. *Nano Lett.* 10, 4738–4741. doi: 10.1021/nl1032556
- Zhou, G., Chang, J., Pu, H., Shi, K., Mao, S., Sui, X., et al. (2016). Ultrasensitive mercury ion detection using DNA-functionalized molybdenum disulfide nanosheet/gold nanoparticle hybrid field-effect transistor device. *ACS Sensors* 1, 295–302. doi: 10.1021/acssensors.5b00241
- Zhuang, J., Fu, L., Tang, D., Xu, M., Chen, G., and Yang, H. (2013). Target-induced structure-switching DNA hairpins for sensitive electrochemical monitoring of mercury (II). *Biosens. Bioelectron.* 39, 315–319. doi: 10.1016/j.bios.2012.07.015

**Conflict of Interest Statement:** The authors declare that the research was conducted in the absence of any commercial or financial relationships that could be construed as a potential conflict of interest.

Copyright © 2018 Tu, Gan, Liang, Hu, Wang, Ren, Sun, Wan and Wang. This is an open-access article distributed under the terms of the Creative Commons Attribution License (CC BY). The use, distribution or reproduction in other forums is permitted, provided the original author(s) and the copyright owner(s) are credited and that the original publication in this journal is cited, in accordance with accepted academic practice. No use, distribution or reproduction is permitted which does not comply with these terms.